Progress In Electromagnetics Research C, Vol. 110, 151–165, 2021

A Dynamic Wireless Power Transfer Using Metamaterial-Based Transmitter

Jiropast Suakaew and Wanchai Pijitrojana*

Abstract—Dynamic Wireless Power Transmission has attracted attention in the research area due to its safety, convenience, and automation. However, the major limitation in achieving this vision is its working distance. In this paper, the metamaterial (MM) based transmitter WPT with zero permeability is presented and compared with an inductive WPT system. The comparative simulations and experimental investigations validate the effectiveness of the proposed design. The system efficiencies are determined at the distances of 8 cm, 11 cm, and 16 cm between the transmitter and receiver (SAE J2954) with an operating frequency of 20 kHz. The power transfer efficiency (PTE) of the WPT system using an inductive transmitter and the WPT system using an MM-based transmitter is shown as 85/87%, 65/70%, 45/65%, respectively. The PTE of the MM-based transmitter is 64% higher than an inductive transmitter at a 16 cm distance. The robot without a battery moves dynamically along the track with the MM-based transmitter underneath. The results show that the power transfer efficiency of the MM-based transmitter is considerably higher than that of the inductive transmitter.

1. INTRODUCTION

Wireless power transfer (WPT) technology makes it possible to supply power through an air gap between the transmitter and receiver without using any wired connection. Wireless charging can be useful in a wide range of applications such as portable devices, medical implants, factory robots, and all-electric vehicles (AEVs) [1–5]. All-electric vehicles are considered one of the leading solutions to reduce the use of fossil fuel and production of air pollution. However, the main all-electric power sources of the all-electric vehicles come from batteries. Therefore, all-electric vehicles (AEVs) run only on electricity. Most all-electric vehicles have all-electric ranges of 80 to 100 miles, while a few luxury all-electric vehicles have ranges up to 250 miles. When the battery is depleted, it can take 30 minutes (with fast charging system) up to nearly a full day to recharge it. This depends on the type of the charging system and the battery. Thus, all-electric ranges and charging time are considered the major issues of all-electric vehicles.

Power transfer efficiency (PTE) is one of the basic terms in WPT technology. To enhance the PTE at a relatively large distance between the transmitter and receiver, several methods have been proposed. An impedance-matching mechanism, repeaters, metamaterial slab between the transmitter and receiver, and magnetically coupled resonators have been considered in the WPT systems [6–9] to increase the power transfer distance and efficiency. A resonant coupling system uses a pair of coupled coils with an additional capacitor, in which the transmitter (Tx) and receiver (Rx) coil operate at the same resonant frequency. The WPT system using resonant coupling schemes enables the energy to transmit highly efficiently over a considerable distance compared to inductively coupled schemes [10–14]. The resonant coil can be directly powered to an excitation source or through inductive coupling. However, most of the

Received 20 January 2021, Accepted 15 February 2021, Scheduled 23 February 2021
* Corresponding author: Wanchai Pijitrojana (pwanchai@engr.tu.ac.th).
The authors are with the Department of Electrical and Computer Engineering, Thammasat University, Klongluang, Pathumthani 12121, Thailand.

WPT systems, which are resonant and inductive coupling schemes, are short-range scheme. It means that the power transfer distance of the WPT system is less than the dimension of the transmitter coils. The applications of the WPT systems are such as the charger of battery-powered automobiles on the highway, warehouse robots, and the wireless power transfer system for elevators that move continuously along the track.

Metamaterials for wireless power appliances show the achievability to advance the range and flexibility of WPT systems. Metamaterials are a new brand of synthetic objects composed of engineered structures having unique characteristics, such as evanescent wave amplification and negative refractive index. Moreover, several applications show that these artificial materials are able to use in the ranges from optical frequencies to radio frequencies [15]. With a property to increase the power transfer efficiency, metamaterials are also used in adaptive charging to increase the operating range of systems, farther distance, and allowance misalignment tolerance for electronic or implantable devices [16]. The in-between MM slab is placed between the Tx and Rx coils to enhance the power transfer efficiency of the system, which is used commonly to increase the transfer distance and power efficiency [17–21].

In this paper, we propose to implement a transmitter based on magnetic metamaterials. The WPT system in this paper is a middle-range scheme. We are also able to overcome the limitations of the in-between metamaterials for the Tx and Rx coils [22–25]. The applications of our system are such as the practical miniaturized devices, the devices achievability to advance the distance, and flexibility of dynamic WPT systems. A capacitor-loaded to the coil is also placed on the transmitter side to reduce the system size. MM-based transmitter is a promising solution for its compact construction, low frequency, and low losses.

2. TRANSMITTING MAGNETIC METAMATERIAL CONCEPTS

2.1. Magnetic Field Considerations

The properties of the conventional materials such as "permittivity ε" and "permeability μ" are derived from the macroscopic response of "electric field E" and "magnetic field H," which represents an average response of the system. At the same time, metamaterials structure is composed of several subunits in which each subunit is much smaller than the wavelength of the system and acts like an atom in the macroscopic scale, so the effective "permittivity ε" and "permeability μ" depend upon the structure of the metamaterials. Therefore, a suitable arrangement can be designed to have electromagnetic properties for various applications [26]. Metamaterials can mainly be used in controlling the near field directions; however, the closer fields will interact with individual units mathematically represented by "effective permittivity ε_{eff}" and "effective permeability μ_{eff}". The structure shows that it has positive, zero, and negative permeability. The magnetic boundary condition has been changed by the value of relative permeability, which leads to Equation (1). Fig. 1 shows magnetic field lines of metamaterials with positive and zero permeability, which bends the magnetic field direction vector to a desirable angle [27–29].

$$\frac{\tan\theta_1}{\tan\theta_2} = \frac{\mu_1}{\mu_2} \tag{1}$$

Figure 2 shows the 3-D electromagnetic field simulation of an inductive and MM-based transmitter WPT systems. The magnetic field intensity from the Tx to the Rx coils is more concentrated on the

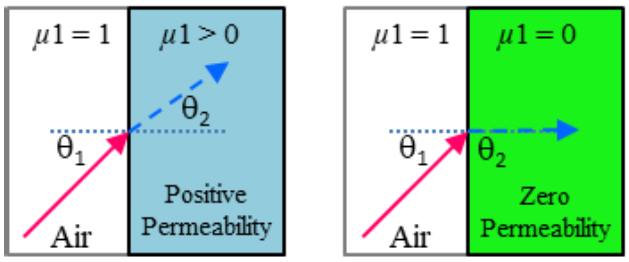

Figure 1. Magnetic field lines of metamaterials having positive and zero permeability.

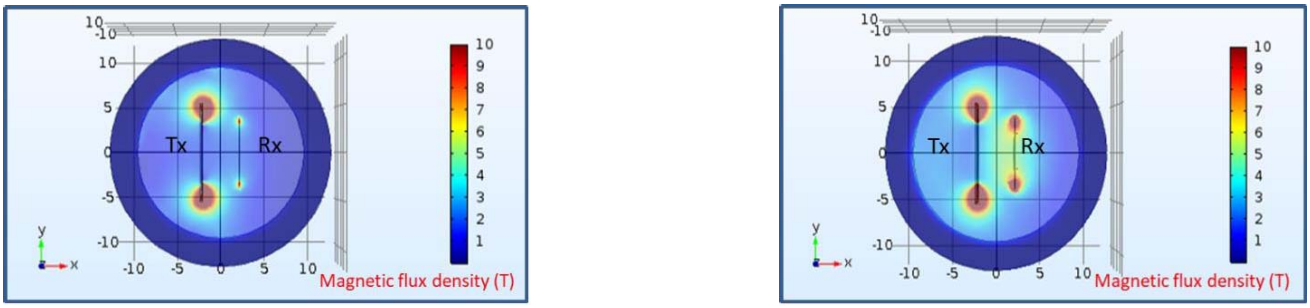

(a) (b)

Figure 2. Simulation results of the magnetic field intensity from Tx to Rx coil. (a) An inductive WPT system. (b) MM-based transmitter having a zero permeability WPT system.

Rx side of Fig. 2(b), the MM-based transmitter due to the magnetic boundary conditions.

Utilizing the coupled-mode concept developed magnetic field enhancement [30], which can be expressed by Equation (2), "m" is the total number of unit cells. K_{kn} is the coupling factor among unit cells related to the coupling coefficient k, $K_{kn} = k\omega_o/2$, in which $\omega_o = 1/\sqrt{LC}$ is the resonant frequency of a single MM. Γ_n is the intrinsic decay, and the radiation losses are presented by the model,

$$\frac{da_n(t)}{dt} = -(j\omega_o + \Gamma_n)\, a_n + j\sum_{k=1}^{m,\,k\neq n} K_{kn} a_k(t), \quad n = 1, ..., m, \tag{2}$$

The operating frequency is powered by the RF magnetic field produced by the Tx coil. The induced magnetic field contains two components, along the axial direction and radial direction. Only the magnetic field component along the axial direction of the coil contributes to the magnetic field enhancement and can be calculated as Equation (3):

$$B_Z = \frac{\mu_o n I_0 a}{4\pi l}\int_{-1/2}^{1/2} \cos\frac{\pi z'}{l}\int_0^{2\pi} A d\varphi' dz', \quad A = \frac{\alpha - \rho\cos\varphi'}{\left[\rho^2 - 2a\rho\cos\varphi' + a^2 + (z-z')^2\right]^{3/2}} \tag{3}$$

I_0 is the amplitude of the current in the unit cells; n is the number of turns; 'l' and 'a' are the height and radius of the MM, respectively, while $\cos\pi z'/l$ reflects the current distribution near the MM, whereas the polar coordinate target points are z and ρ.

The simulation analyses have been conducted to validate this theoretical concept. The enameled Lize copper wire parameters are shown in Table 1.

The simulation setup of operating frequency and magnetic field enhancement behavior are derived between the adjacent unit cells, shown in Fig. 3(a). Fig. 3(b) characterizes the operating frequency and magnetic field enhancement response of the adjacent cell space (d) to cell size (D), d/D ratio.

Table 1. The coil parameters.

No	Term	Dimensions
1	MMi/RX Coil	33 AWG Lize wire, Copper
2	Coil strands	38
3	Coil turn	27 turns
4	Coil OD	Outside diameter, 8 cm
5	Coil ID	Inside diameter, 2 cm
6	Coil inductance	140 µH (internal coil)
7	Capacitance	0.47 µF (external C)
8	Coil Resistance	135 mΩ

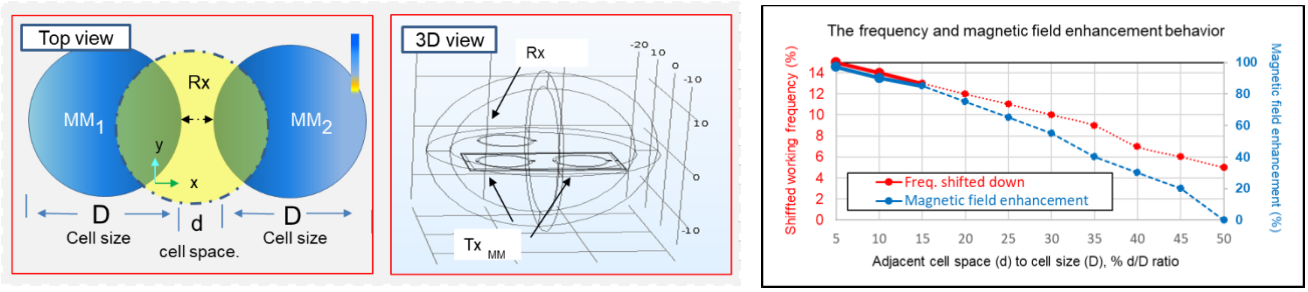

(a) (b)

Figure 3. Parameter studies and variation in response of the adjacent cell space to cell size. (a) Simulation set-up of adjacent MM units cell. (b) Characterize the working frequency and magnetic field enhancement.

The operating frequency and magnetic field enhancement is gradually shifted when the ratio d/D is up to 15%, but is significantly affected if it goes beyond 15% d/D value. The mutual coupling from neighboring MM affects the total inductance, and the operating frequency shifts down.

2.2. Transmission Efficiency in the Variation of MM Unit Cells Structures

The periodic boundary condition simulation is conducted between the Tx and Rx coils with different MM unit cells structures. The design, structure, size, and orientation are shown in Fig. 4(a).

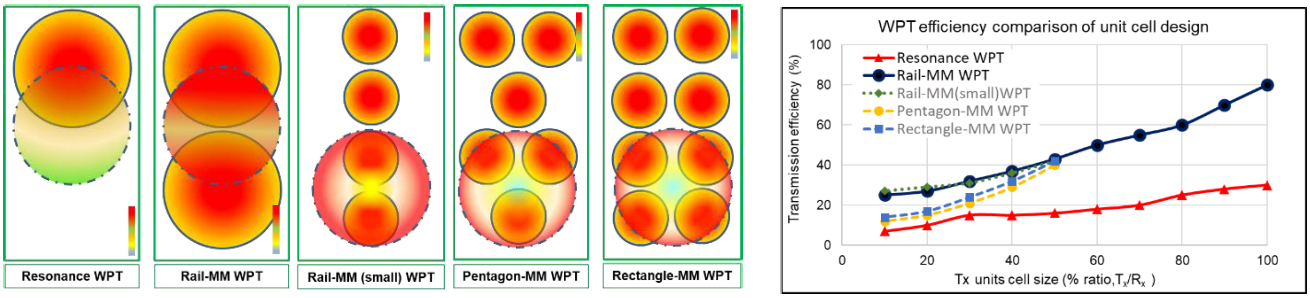

(a) (b)

Figure 4. (a) Simulation set-up of transmission efficiency with cell structures, sizes, and orientations. (b) Simulation results of the S-parameter transmission efficiency.

Figure 4(b) indicates the efficiencies of the WPT system with different cell structures. The graph shows the improvement that occurs with an enlarging size of the Tx coil. Therefore, Tx coil's size design is limited to the Rx coil's size. Different colors show the magnetic field strength developed from the periodic boundary condition simulation. The rail MM's structure shows higher magnetic field strength than other designs, including rectangle and pentagon geometries, which are the simulation limit to 50% fitting with Rx coil's size. The rail MM's structure by the S-parameter transmission efficiency improves up to 50% compared to the inductive resonance system.

3. TRANSMITTER DESIGN

3.1. Magnetic Metamaterial Considerations for the Transmitter

The operating frequency and relative permeability are essential parameters that need to be considered in designing a metamaterial structure. Nicolson-Ross-Weir (NRW) method [31] is used to find the real

Table 2. Terms of Nicholson-Ross-Weir conversion process.

S.no	Term	Abbreviations
1	S_{11}	Reflection, S-parameter
2	S_{21}	Transmission, S-parameter
3	Γ	Reflection coefficient
4	T	Transmission coefficient
5	μ	Permeability
6	λ_o	Free space wavelength
7	λ_c	Cutoff wavelength
8	L	Material length

and imaginary permeabilities, which can be expressed by Equations (4)–(9), and the parameters used in these equations are defined in Table 2. The extracted real and imaginary permeability values are derived from the parameter extraction technique based on S-parameter reflection and transmission.

$$\mu = \mu_r \mu_o \tag{4}$$

The normalized term could be derived from the measured S-parameters:

$$X = \frac{S_{11}^2 - S_{21}^2 + 1}{2S_{11}} \tag{5}$$

with mathematical manipulation, the reflection coefficient can be deduced as:

$$\Gamma = X \pm \sqrt{X^2 - 1} \tag{6}$$

The transmission coefficient can be written as:

$$T = \frac{S_{11} + S_{21} - \Gamma}{1 - (S_{11} + S_{21})\,\Gamma} \tag{7}$$

where λ_o is the free space wavelength, and λ_c is the cutoff wavelength

$$\frac{1}{\Lambda^2} = \left\{ \frac{\varepsilon_r * \mu_r}{\lambda_0^2} - \frac{1}{\lambda_c^2} \right\} = - \left\{ \frac{1}{2\pi L} \ln\left(\frac{1}{T}\right) \right\}^2 \tag{8}$$

By equating this equation, the permeability can be obtained:

$$\mu = \frac{1 + \Gamma}{\Lambda\,(1 - \Gamma)\sqrt{\left(\frac{1}{\lambda_0^2} - \frac{1}{\lambda_c^2}\right)}} \tag{9}$$

Substituting the coil geometry from Table 1 with the rail MM's structure from Fig. 4(a) into NRW's method, the estimation of the relative permeability is efficient in designing the initial structure of the metamaterial. The extracted permeability values for the MM-based transmitter are shown in Figs. 5(a)–(b), having extracted real (blue) and imaginary (orange) permeability values. The resonance frequency of the conventional resonator ($L + C$) is 19.8 kHz, while the resonance frequency of the proposed metamaterial resonator is a different operating frequency of 20 kHz. Because the proposed metamaterial resonator comprises several subunits, the mutual coupling inductance of the neighboring MM subunit affects the total inductance. It consequently causes different effective operating frequencies.

Ideally, MM coil's design and structure with a negative or zero relative permeability affect the magnetic field lines direction of the Tx coil by bending it towards the Rx coil. The metamaterials with controlled permeability are adopted into the WPT coil module because the vector direction of the magnetic field from the Tx coil can be controlled, in which the system increases the magnetic flux density. To increase Q, enameled Lize copper wire is used for the metamaterial coil's design, operating at the power transfer frequency 20 kHz. The value of the inductance and resistance of the metamaterial coils are approximately 140 µH and 135 mΩ, respectively. The quality factor $Q = \omega L/R$ of the metamaterial coil is 130. It is considered satisfactory for the WPT system.

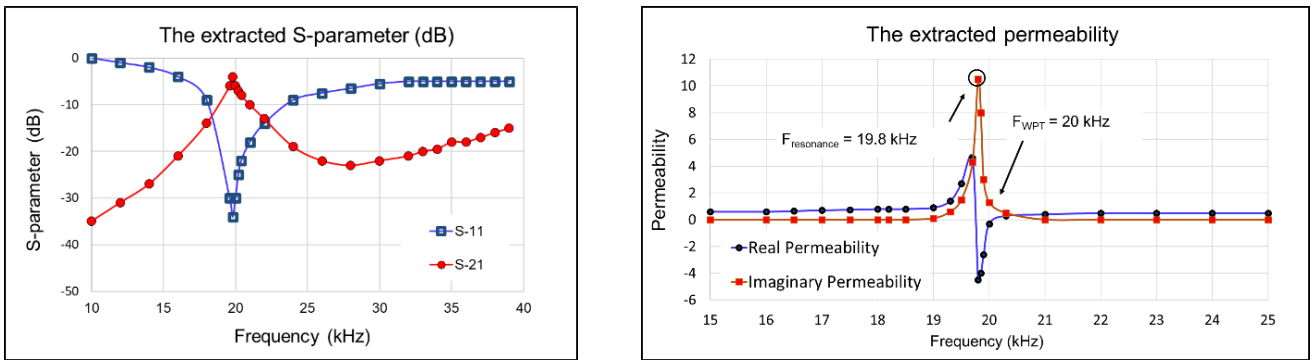

(a) (b)

Figure 5. Transmission and reflection coefficients. (a) The transmission coefficient, S_{21}, and the reflection coefficient, S_{11}. (b) Extracted real (blue) and imaginary (orange) permeability values.

3.2. Magnetic Metamaterial Implementations for the Transmitter

The lumped concept can engage in describing the corresponding self-inductance of isolated unit cells by Equations (10)–(12) [32], and inductance L_{total} and capacitance C_{total} of the MM unit cell are 140 µH and 0.47 µF, respectively. Figs. 6(a)–(b) show an array of metamaterial structures with the inner diameter D_i, an outer diameter D of the conductor, and S is the spacing between the turns. The effect of the ground plane on the inductance value can be reduced by keeping $S < W$. Terms of the lumped circuit and the parameters used in these equations are defined in Table 3.

$$L_{\text{total}} = \frac{\mu_0 n^2 D_{av} A_1}{2}\left[\ln\frac{A_2}{\rho} + A_3\rho + A_4\rho^2\right], \quad \rho = \frac{D_0 - D_i}{D_0 + D_i} \tag{10}$$

$$C_{\text{total}} = C_{\text{intrinsic}} + C_{\text{external}} \tag{11}$$

$$C_{\text{intrinsic}} = 3.5 * 10^{-5} D_0 + 0.06 \tag{12}$$

$$\omega = \frac{1}{\sqrt{LC}} \tag{13}$$

The Tx coil's operating frequency is calculated from Equation (13), 20 kHz. Usually, the Tx coil determines the system's power transfer level, efficiency, and overall performance. The MM consists of Litz spiral winding with an outer diameter and a cell distance of 8 cm and 2 cm, respectively. A compensator capacitance determines the working frequency and low sensitivity to the external objects, effective inductance and capacitance of 140 µH and 0.47 µF, respectively. The efficiency improvement of the magnetic coupling between the Tx coil and MM unit cells is that only a small current is needed for the source coil to induce a large current in the MM-based transmitter, which generates an enhanced magnetic field to transfer the power to the Rx coil. When the large current of the Tx coil does not flow through the primary source's resistance, a small power loss can be achieved in the driving circuit.

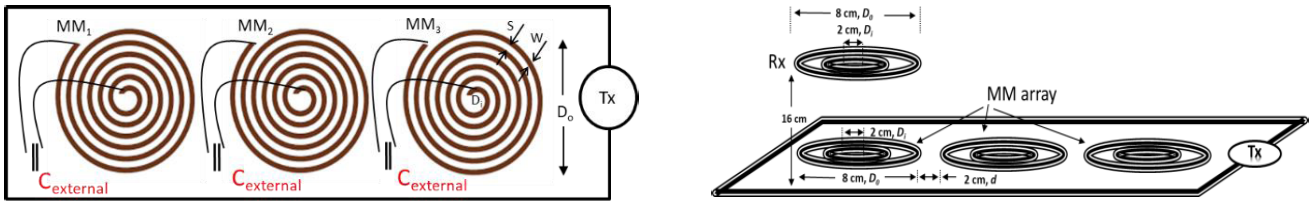

(a) (b)

Figure 6. An array of 3 unit cells of the enameled Lize copper coil with a capacitor loading to the MM-based transmitter. (a) The top view. (b) The side view.

Table 3. Terms of lumped circuit.

S.no	Term	Abbreviations
1	C_{total}, $C_{\text{intrinsic}}$	Capacitance, μF
2	A_1	Geometry coefficient, 1.00
3	A_2	Geometry coefficient, 2.46
4	A_3	Geometry coefficient, 0
5	A_4	Geometry coefficient, 0.2
6	D_o	Inductor's Outside diameter, 8 cm
7	D_i	Inductor's Inside diameter, 2 cm
8	L_{total}	Inductance
9	n	Number of coil turns
10	S	Spacing between turns
11	W	Coil width
12	ρ	The fill ratio
13	μ	Material Permeability

4. RECEIVER DESIGN

In this paper, a series-series SS topology compensator is used by reflected impedance theory. The Rx side of a system needs a compensation capacitance to eliminate the imaginary part [33, 34]. Various network topologies can calculate the compensated capacitances to ensure the maximum real value and minimum imaginary value $(\omega L_{Rx_{\text{intrinsic}}} + X_{\text{load}})^2$. SS topology is independent of the coupling coefficient and load conditions, and the reflected reactance equals zero on the primary side.

The parameters are listed in Table 4, where ω_0 is the resonant frequency, M the mutual inductance between the coils and L_{Tx}, and L_{Rx} the Tx and Rx coil's self-inductance. The coils resonate at the resonance frequency, $f_o = f_{Tx} = f_{Rx}$, and can also be expressed by Equation (14).

$$f_o = \frac{1}{2\pi\sqrt{LC}} \tag{14}$$

Table 4. Terms of series-series topologies.

Parameter	Secondary Quality factor	Reflected resistance	Primary capacitance
SS topologies	$\frac{\omega_O L_s}{R}$	$\frac{\omega_o^2 M^2}{R}$	$\frac{C_{Tx} L_{Rx}}{L_{Tx}}$

The receiver side of a system contains a coil, a conditioning circuit in the form of a rectifier, a filter, and a controllable load. The receiver compensation is tuned at the frequency of the field emitted by the Tx coil and reflects resistive and reactive impedances to the Tx coil. The resistive component is a function of the receiver loading and corresponds to the load's power. The reactive part is typically unwanted, which effectively detunes the resonant coil on the transmitter side.

5. SYSTEM AND EXPERIMENTAL SET-UP

5.1. System Efficiency

This section accesses the MM-based transmitter and determines the key factors that target maximum power transfer frequency. Fig. 7 shows the equivalent circuit of the MM-based transmitter and receiver coils.

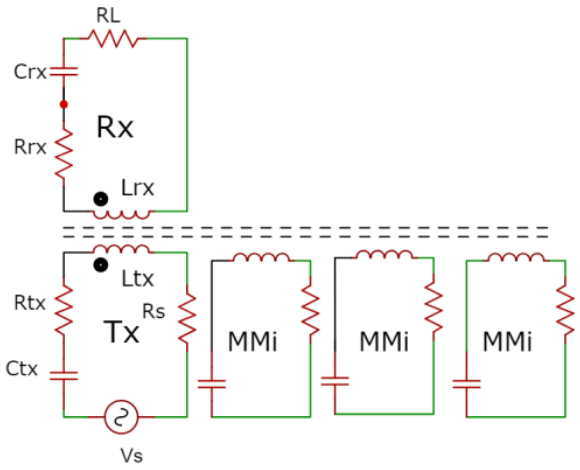

Figure 7. Circuit diagram for experimental verification.

MM cell is employed as the main coil on the transmitter side connected to the resonant capacitor [35–37]. The system is excited by the Tx coil. The energy is transferred to a load. Due to the large transfer distance, the Tx and Rx coils' magnetic coupling is considered negligibly small compared to the MM cell's coupling to the Rx coil. The transmitting MM is excited at the resonant frequency, thus ($X_{Tx} = X_{MMi} = X_{Rx} = 0$), and the lumped circuit formulas are given by Equations (15)–(17) [38, 39].

$$(\mathbf{R}_s + \mathbf{R}_{TX})\mathbf{I}_{TX} + j\omega M_{TxMMi}\mathbf{I}_{MMi} = \mathbf{V}_s \tag{15}$$

$$j\omega M_{TxMMi}\mathbf{I}_{TX} + \mathbf{R}_{MMi}\mathbf{I}_{MMi} + j\omega M_{RxMMi}\mathbf{I}_{RX} = 0 \tag{16}$$

$$j\omega M_{RxMMi}\mathbf{I}_{MMi} + (R_L + R_{RX})\,\mathbf{I}_{Rx} = 0 \tag{17}$$

The terms used in lumped circuit elements are shown in Table 5.

Table 5. Terms of lumped circuit.

S.no	Terms	Abbreviations
1	R_s	Source resistance
2	R_{TX}	Transmission coil resistance
3	R_{MMi}	Metamaterial coil resistance
4	R_{RX}	Receiving coil resistance
5	M_{MMiTX}	Mutual inductance of the Tx coil and metamaterial coils
6	M_{RXMMi}	Mutual Inductance of Rx coil and metamaterial coil
7	I_{TX}	Transmission coil current
8	I_{RX}	Receiving coil current
9	I_{MMi}	Metamaterial coil current
10	η_{Total}	Total Efficiency
11	η_{Tx}	Transmission coil efficiency
12	η_{MMi}	Metamaterial coil efficiency
13	η_{RX}	Receiving coil efficiency

R_{TX} is the Tx coil's parasitic resistance, R_s the source resistance, $R_s + R_{Tx}$ the Tx coil's resistance, $R_L + R_{Rx}$ the receiver's resistance, R_L the load resistance, and R_{Rx} the receiver coil's parasitic resistance. The system efficiency can be expressed by Equations (18)–(23).

$$\eta_{Total} = \eta_{Tx}\eta_{MMi}\eta_{Rx} \tag{18}$$

Table 6. Terms of reflected resistance.

S.no	Terms	Abbreviations
1	R_{TxMMi}	Reflected resistance from metamaterial coil to Tx coil
2	R_{RxMMi}	Reflected resistance from receiving coil to metamaterial coil

The terms used in reflected resistances are shown in Table 6.

$$\eta_{Tx} = \frac{R_{ETx}}{R_S + R_{Tx} + R_{ETx}} \tag{19}$$

$$R_{TxMMi} = \frac{\omega^2 M_{TxMMi}^2}{R_{MMi} + R_{RxMMi}} \tag{20}$$

$$R_{RxMMi} = \frac{\omega^2 M_{RxMMi}^2}{R_L} \tag{21}$$

$$\eta_{MMi} = \frac{R_{RxMMi}}{R_{MMi} + R_{RxMMi}} \tag{22}$$

$$\eta_{Rx} = \frac{R_L}{R_{Rx} + R_L} \tag{23}$$

Equation (23) expresses the energy efficiency of the receiver η_{Rx}, where the reflected resistance MMi to Rx is R_{RxMMi}. The principal importance behind this effectiveness improvement is that the offered MM-based transmitter uses the magnetic coupling between Tx and MM so that a large current in the MM is induced by a small current Tx, generating an enhancement of the power transfer magnetics flux of MM to Rx. The source resistance of the power source has a small current flow through it, and the driving circuit has a much smaller loss.

5.2. Experimental Set-up and Results

In this research work, an MM-based transmitter is designed entirely in the system, enhancing the magnetic field. The full power bandwidth of the MD30C inverter board PWM is 20 kHz. The experiment layout is shown in Fig. 8, which includes an H-Bridge MD30C power driver, an oscilloscope having a 2-channel probe for AC power measurement, a wattmeter for DC power measurement of current and voltage, an HF signal generator having a specification of 5v p-p, an Arduino component for getting the square wave, and an AC to DC converter with a specification of 22–32 V and a maximum current of 80 A.

The MD30C board is an invertor with PWM control, modified to operate with a signal generator, and the power supply capacity is up to 80 A peak and 30 A continuously. The signal generator is connected to PWM on the MD30C board to be an HF source of power supply to the Tx coil shown in Fig. 9.

The transmission efficiencies between the Tx and Rx coils of the inductive and MM-based transmitter WPT systems have been compared. Figs. 10(a)–(b) show that the MM-based transmitter has the best performance at the air gaps of 8, 11, and 16 cm. The self and mutual inductance L and intrinsic capacitance C of each system have been dominant in the operating frequency by their designed structure. An optimized operating frequency has been used to compare the performance and get each system's maximum efficiency.

Different measurements are taken at nine different positions, as shown in Fig. 11–Fig. 12, based on the receiver coil's location underneath the moving robot.

These positions are 1) Right before alignment with the first MM coil, edge to edge. 2) 50% aligned with the first MM coil. 3) Perfectly aligned with the first MM coil. 4) 50% misaligned with the first MM coil towards the second MM coil. 5) Perfectly aligned with the second MM coil, position. 6) 50% aligned with the second MM coil. 7) Perfectly aligned with the third MM coil. 8) 50% misaligned with the third MM coil. 9) Right after alignment with the third MM coil, edge to edge.

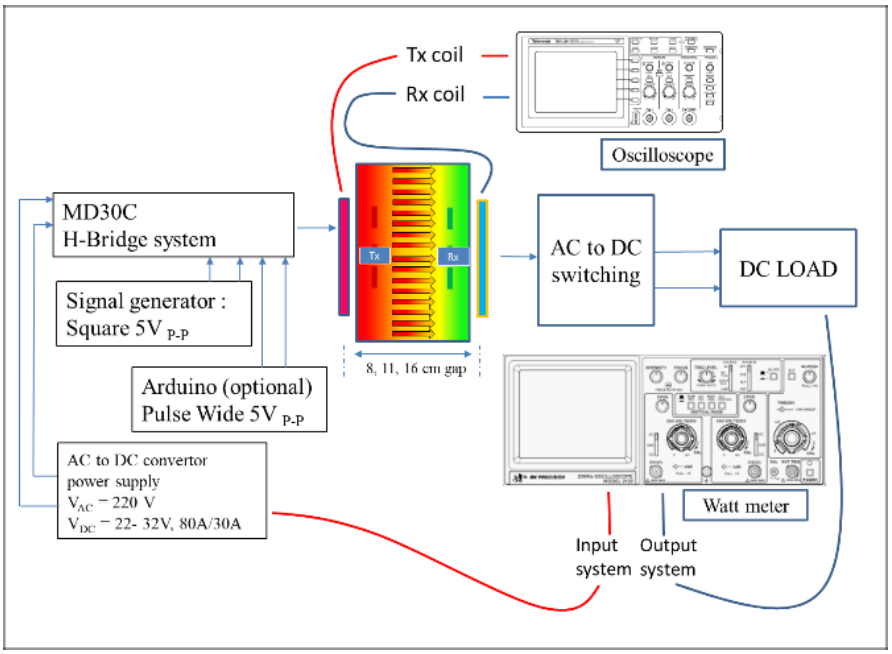

Figure 8. Experimental setup for the WPT system.

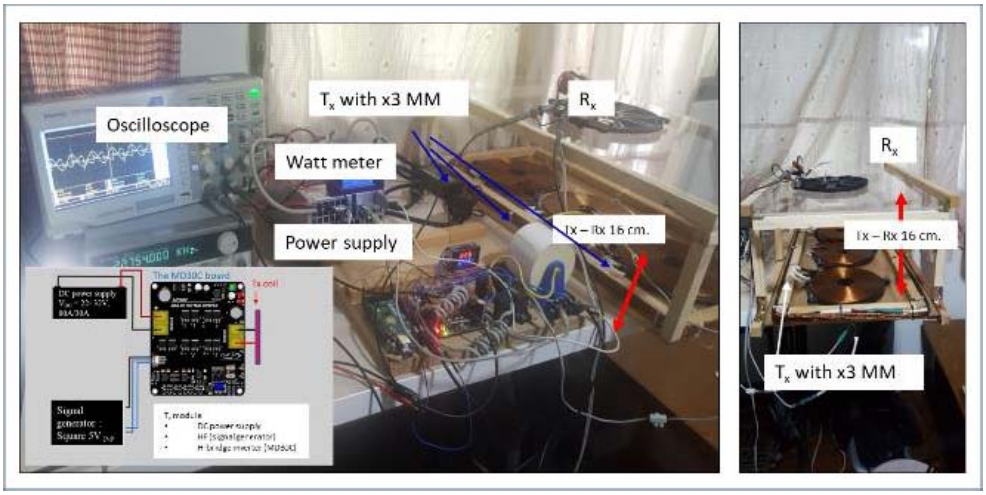

Figure 9. Experimental setup of the MM-based transmitter. Tx to Rx coil distance is 16 cm.

The coupling efficiencies are measured and compared with an inductive and MM-based transmitter WPT systems. A DC wattmeter is used to measure the power efficiency at the power supply to the load, and an oscilloscope is used to measure the power efficiency from Tx to Rx coils.

The power transfer efficiencies of the Rx coil at different positions are shown in Fig. 13. An optimized frequency of 20 kHz is excited about the MM-based transmitter WPT system. PTE shows the inductive and MM-based transmitter WPT systems of 85/87%, 65/70%, and 45/65%. PTE of the MM-based transmitter is 64% higher than an inductive WPT at a 16 cm distance. A slight fluctuation and different efficiency patterns at different locations on the Rx, as the Rx travels from one edge to the other edge, is affected by adjacent MM cells' spacing. On the other hand, at the Rx, different efficiencies and fluctuations can be improved by tweaking the operating frequencies contingent on the Rx coil location, as plotted in Fig. 3. A data link can be set up for the Tx and Rx coil system in a

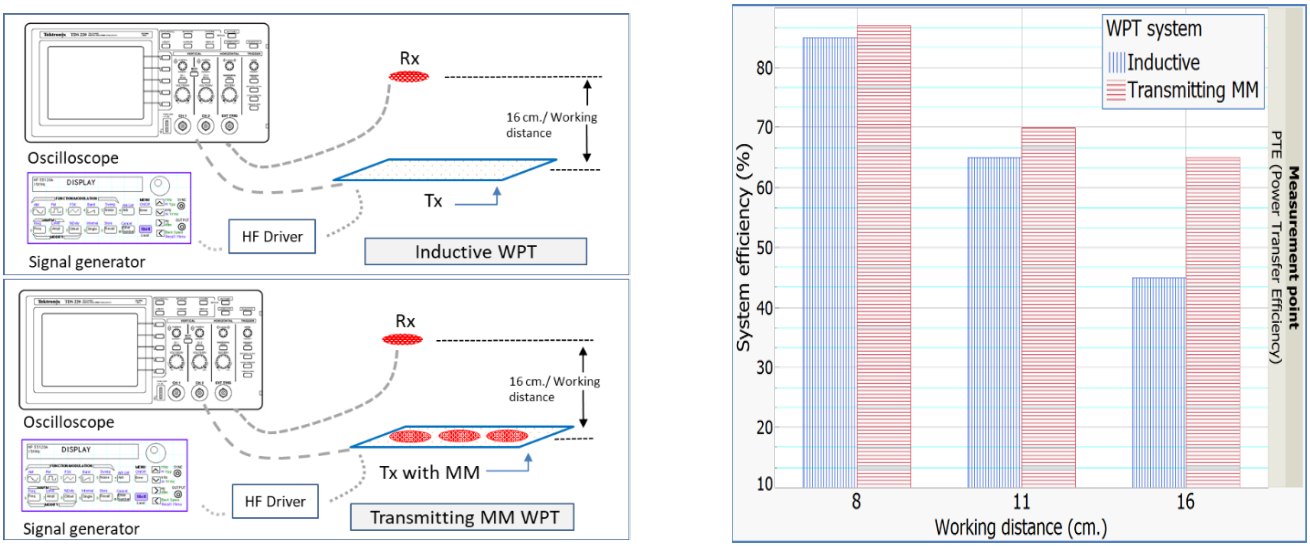

Figure 10. (a) An experiment diagram of an inductive WPT, the MM-based transmitter. (b) Transmission efficiencies of the inductive system, and the MM-based transmitter at an air gap 8, 11, and 16 cm.

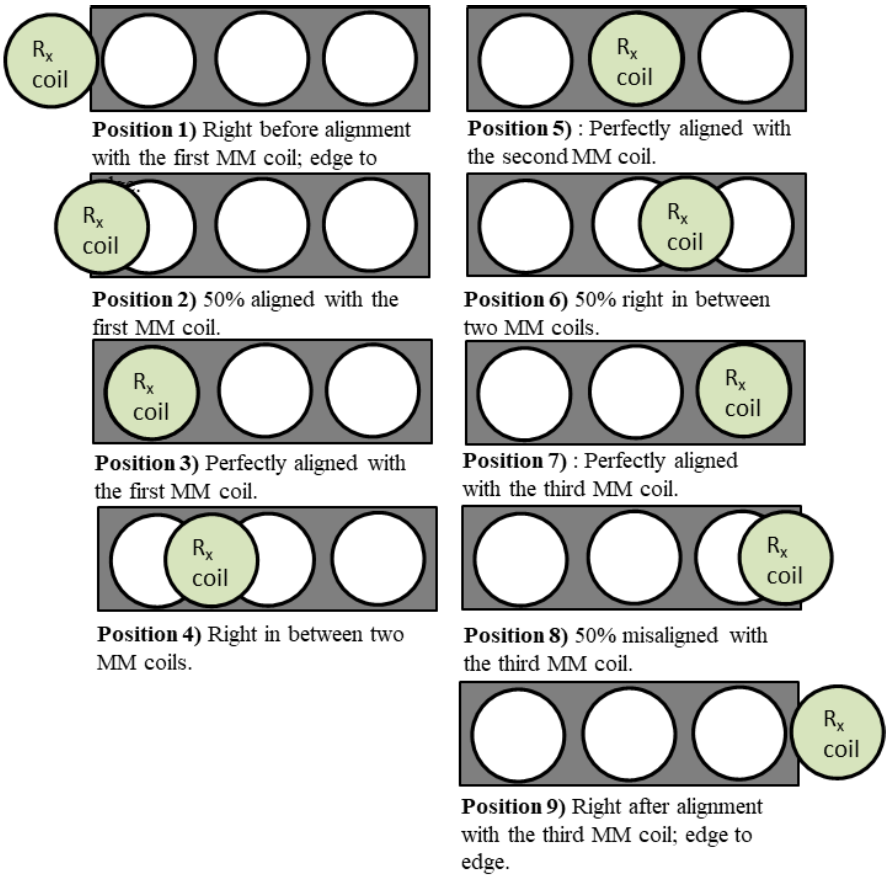

Figure 11. Set-up the Rx as a function of location. The Rx passes by the Tx, and measurements are taken at nine different position.

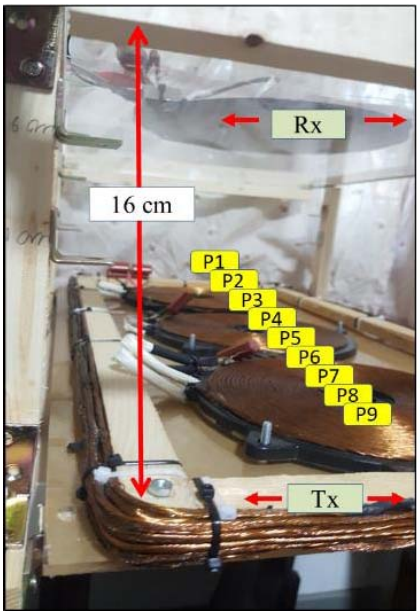

Figure 12. Experimental setup of the system and their measurements taken at nine different positions.

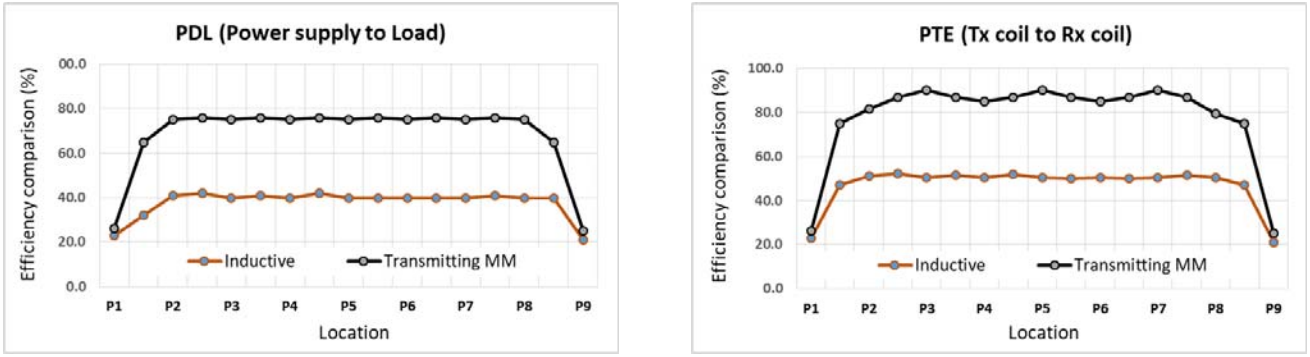

Figure 13. WPT efficiency. (a) From the power supply to the load. (b) From the Tx coil to the Rx coil.

closed-loop stabilizer. In [40], the authors present a robust and efficient WPT by using a switch-mode implementation. However, this approval requires an amplifier circuit with current-sensing feedback. It can be useful and flexible for future work of wireless power delivery solutions.

6. THE DYNAMIC WPT EXPERIMENTAL SET-UP

An experiment is performed to demonstrate the flexibility of the dynamic WPT. The system operates at an operating frequency of 20 kHz with a robot running on a road made up of plastic and wood. The dimensions of the road are 20 cm $*$ 120 cm. The MM-based transmitter WPT system used in this experiment is implemented as a unit cell having Litz spiral winding, and the number of turns is 28 with an inductance and a capacitance of 140 μH and 0.47 μF, respectively. The outer diameter of an MM unit cell is 8 cm while the inner diameter is 2 cm, with a horizontal distance between MM is 2 cm. The Tx system is located beneath the road with HF power delivered to the array of the MM-based transmitter WPT system. The Tx and Rx coil distance is 16 cm. Robot batteries are disconnected and supplanted

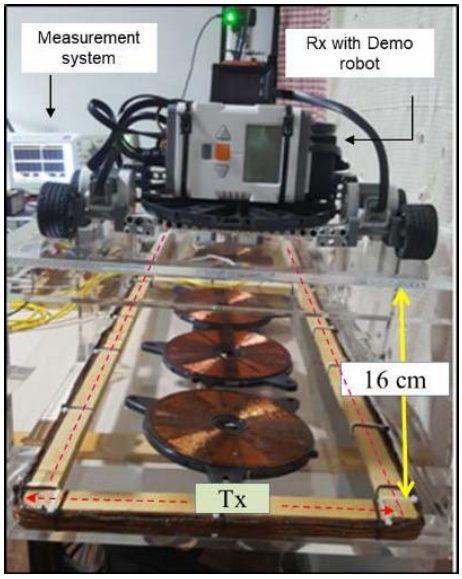

Figure 14. Dynamic WPT experiment set up of the MM-based transmitter WPT system. The system is delivered the wireless power to the receiver that is the robot set traveling on the road.

by a module for power conversion to deliver power to the robot. Fig. 14 shows the experiment setup of the system in which the robot set can move continuously along the road.

7. CONCLUSION

We propose an MM-based transmitter WPT system having zero permeability property derived from the sub-units. An MM-based transmitter is implemented on the transmitter side to increase the dynamic wireless charging system efficiency, enhancing the system's magnetic field to overcome the limitations of the in-between metamaterials for longer distances. PTE shows the inductive and MM-based transmitter WPT systems of 85/87%, 65/70%, and 45/65%. PTE of the MM-based transmitter is 64% higher than an inductive WPT at a 16 cm distance. Moreover, wireless charging can be used for battery-powered vehicles, elevators, and warehouse robots that can travel continuously along the road.

REFERENCES

1. Kim, C.-G., D.-H. Seo, J.-S. You, J.-H. Park, and B. H. Cho, "Design of a contactless battery charger for cellular phone," *IEEE Trans. Ind. Electron.*, Vol. 48, No. 6, 1238–1247, Dec. 2001.
2. Jabbar, H., Y. S. Song, and T. T. Jeong, "RF energy harvesting system and circuits for charging of mobile devices," *IEEE Trans. Consum. Electron.*, Vol. 56, No. 1, 247–253, Feb. 2010.
3. Shiba, K., A. Morimasa, and H. Hirano, "Design and development of low-loss transformer for powering small implantable medical devices," *IEEE Trans. Biomed. Circuits Syst.*, Vol. 4, No. 2, 77–85, Apr. 2010.
4. Wang, C.-S., O. H. Stielau, and G. A. Covic, "Design considerations for a contactless electric vehicle battery charger," *IEEE Trans. Ind. Electron.*, Vol. 52, No. 5, 1308–1314, Oct. 2005.
5. Madawala, U. K. and D. J. Thrimawithana, "A bidirectional inductive power interface for electric vehicles in V2G systems," *IEEE Trans. Ind. Electron.*, Vol. 58, No. 10, 4789–4796, Oct. 2011.
6. Kiani, M. and M. Ghovanloo, "The circuit theory behind coupled-mode magnetic resonance-based wireless power transmission," *IEEE Trans. Circuits Syst. I Regul. Pap.*, Vol. 59, No. 9, 2065–2074, Sep. 2012.

7. Hui, S. Y. R., W. Zhong, and C. K. Lee, "A critical review of recent progress in mid-range wireless power transfer," *IEEE Trans. Power Electron.*, Vol. 29, No. 9, 4500–4511, Sep. 2014.
8. Lee, K. and S. H. Chae, "Power transfer efficiency analysis of intermediate-resonator for wireless power transfer," *IEEE Trans. Power Electron.*, Vol. 8993, 1–1, Apr. 2017.
9. Zhong, W. X., et al., "A methodology for making a three-coil wireless power transfer system more energy efficient than a two-coil counterpart for extended transfer distance," *IEEE Trans. Power Electron.*, Vol. 30, No. 2, Feb. 2015.
10. Kim, S.-H., Y.-S. Lim, and S.-J. Lee, "Magnetic resonant coupling based wireless power transfer system with in-band communication "Gangwon-do in Korea"," *Department of Electronics Engineering, Ewha Woman's Univ. Journal of Semiconductor Technology and Science*, Vol. 13, No. 6, Dec. 2013.
11. Rittiplang, A. and W. Pijitrojana, "A low-frequency wireless power transfer using parallel resonance under impedance matching," *Applied Mechanics and Material*, Vol. 781, 410–413, Aug. 2015.
12. Rittiplang, A. and W. Pijitrojana, "Low-frequency wireless power transfer using optimal primary capacitance of parallel resonance for impedance matching," *IJIREEICE*, Vol. 4, No. 1, Jan. 2016.
13. Rittiplang, A., W. Pijitrojana, and K. Daroj, "Low-frequency wireless power transfers using modified parallel resonance matching at complex load," *KKU Engineering Journal*, 184–188, Oct./Dec. 2016.
14. Rittiplang, A. and W. Pijitrojana, "Development of in-motion wireless power transfer test bed platform for wireless electric vehicle charger," *Thammasat International Journal of Science and Technology*, Vol. 22, No. 2, 2017.
15. Wang, B., W. Yerazunis, and K. H. Teo, "Wireless power transfer: Metamaterials and array of coupled resonators," *Proceedings of the IEEE*, Vol. 101, No. 6, 1359–1368, Jun. 2013.
16. Li, L., H. Liu, H. Zhang, and W. Xue, "Efficient wireless power transfer system integrating with metasurface for biological applications," *IEEE Trans. Ind. Electron.*, Vol. 65, No. 4, 3230–3239, Apr. 2018.
17. Wu, Q., Y. H. Li, N. Gao, F. Yang, Y. Q. Chen, K. Fang, Y. W. Zhang, and H. Chen, "Wireless power transfer based on magnetic metamaterials consisting of assembled ultra-subwavelength meta-atoms," *Europhysics Letters, EPL*, Vol. 109, No. 6, 68005, Mar. 2015.
18. Rajagopalan, A., A. K. RamRakhyani, D. Schurig, and G. Lazzi, "Improving power transfer efficiency of a short-range telemetry system using compact metamaterials," *IEEE Transactions on Microwave Theory and Techniques*, Vol. 62, No. 4, 947–955, Apr. 2014.
19. Das, R., A. Basir, and H. Yoo, "A metamaterial-coupled wireless power transfer system based on cubic high-dielectric resonators," *IEEE Trans. Ind. Electron.*, Vol. 66, No. 9, 7397–7406, Sep. 2019.
20. Wang, X., Y. Wang, Y. Hu, Y. He, and Z. Yan, "Analysis of wireless power transfer using superconducting metamaterials," *IEEE Transactions on Applied Superconductivity*, Vol. 29, No. 2, Mar. 2019.
21. Lu, C., X. Huang, C. Rong, Z. Hu, J. Chen, X. Tao, S. Wang, B. Wei, and M. Liu, "Shielding the magnetic field of wireless power transfer system using zero-permeability metamaterial," *IET Journals*, Vol. 2019, No. 16, 1812–1815, 2019.
22. Cho, Y., S. Lee, D.-H. Kim, H. Kim, C. Song, S. Kong, J. Park, C. Seo, and J. Kim, "Thin hybrid metamaterial slab with negative and zero permeability for high efficiency and low electromagnetic field in wireless power transfer systems," *IEEE Trans. Ind. Electron.*, Vol. 60, No. 4, 1001–1009, Aug. 2018.
23. Wang, B., T. Nishino, and K. H. Teo, "Wireless power transmission efficiency enhancement with metamaterials," *Proc. IEEE Int. Conf. Wireless Inf. Technol. Syst.*, Honululu, HI, USA, Aug. 28–Sep. 3, 2010, doi: 10.1109/ ICWITS.2010.5612284.
24. Urzhumov, Y. and D. R. Smith, "Metamaterial-enhanced coupling between magnetic dipoles for efficient wireless power transfer," *Phys. Rev. B*, Vol. 83, 205114, 2011.

25. Wang, B., K. H. Teo, T. Nishino, W. Yerazunis, J. Barnwell, and J. Zhang, "Wireless power transfer with metamaterials," *Proc. Eur. Conf. Antennas Propag.*, 3905–3908, Rome, Italy, Apr. 11–15, 2011.
26. Pendry, J. B., "Negative refraction," *Contemporary Physics*, Vol. 45, No. 3, 191–202, 191–202, Aug. 7, 2006.
27. Cho, Y., et al., "Hybrid metamaterial with zero and negative permeability to enhance efficiency in wireless power transfer system," *IEEE Wireless Power Transfer Conference (WPTC)*, 1–3, Aveiro, 2016.
28. Cho, Y., S. Lee, D.-H. Kim, H. Kim, C. Song, S. Kong, J. Park, C. Seo, and J. Kim, "Thin hybrid metamaterial slab with negative and zero permeability for high efficiency and low electromagnetic field in wireless power transfer systems," *IEEE Trans. Ind. Electron.*, Vol. 60, No. 4, 1001–1009, Aug. 2018.
29. Cho, Y., J. J. Kim, D.-H. Kim, S. Lee, H. Kim, C. Song, S. Kong, H. Kim, C. Seo, S. Ahn, and J. Kim, "Thin PCB-type metamaterials for improved efficiency and reduced emf leakage in wireless power transfer systems," *IEEE Transactions on Microwave Theory and Techniques*, Vol. 64, No. 4, 353–364, Feb. 2016.
30. Duan, G., X. Zhao, S. W. Anderson, et al., "Boosting magnetic resonance imaging signal-to-noise ratio using magnetic metamaterials," *Communication Physics*, Vol. 2, 35, 2019.
31. Luukkonen, O., S. I. Maslovski, and S. A. Tretyakov, "A stepwise Nicolson-Ross-Weir-based material parameter extraction method," *IEEE Antennas and Wireless Propagation Letters*, Vol. 10, 1295–1298, 2011.
32. Bahl, J., *Lumped Elements for RF and Microwave Circuits*, Artech House, Norwood, MA, 2003.
33. Lee, K., Z. Pantic, and S. M. Lukic, "Reflexive field containment in dynamic inductive power transfer systems," *IEEE Trans. Power Electron.*, Vol. 29, No. 9, 4592–4602, Sep. 2014.
34. Zhang, Z., A. Georgiadis, and C. Cecati, "Wireless power transfer," *IEEE Trans. Ind. Electron.*, Vol. 66, No. 2, Feb. 2019.
35. Chen, Y., M. Kung, and K. Lin, "Investigation of hybrid metamaterial for enhancing the efficiency of wireless power transfer systems," *IEEE International Symposium on Antennas and Propagation & USNC/URSI National Radio Science Meeting*, 1093–1094, San Diego, CA, 2017.
36. Senior, D. E. and P. V. Parimi, "Planar wireless power transfer system with embedded magnetic metamaterial resonators," *IEEE International Symposium on Antennas and Propagation (APSURSI)*, 607–608, Fajardo, 2016.
37. Abdolkhani, A. and E. Coca, "Fundamentals of inductively coupled wireless power transfer systems," *Wireless Power Transfer — Fundamentals and Technologies*, 3–26, 2016.
38. Zhong, W. X., et al., " A methodology for making a three-coil wireless power transfer system more energy efficient than a two-coil counterpart for extended transfer distance," *IEEE Trans. Power Electron.*, Vol. 30, No. 2, Feb. 2015.
39. Lee, E., X. Thai, S. Choi, C. Rim, and J. Huh, "Impedance transformers for compact and robust coupled magnetic resonance systems," *IEEE Energy Convers. Congr. Expo.*, 2239–2244, Denver, USA, 2013.
40. Assawaworrarit, S. and S. Fan, "Robust and efficient wireless power transfer using a switch-mode implementation of a nonlinear parity-time-symmetric circuit," *Nature Electronics*, Vol. 3, 273–279, 2020.